Antiproton-deuteron hydrogenic states from a coupled-channel approach

Pierre-Yves Duerinck [*]

Physique Nucléaire Théorique et Physique Mathématique, C.P. 229, Université libre de Bruxelles (ULB), B-1050 Brussels, Belgium
and IPHC, CNRS/IN2P3, Université de Strasbourg, 67037 Strasbourg, France

Rimantas Lazauskas [†]

IPHC, CNRS/IN2P3, Université de Strasbourg, 67037 Strasbourg, France

Jérémy Dohet-Eraly [‡]

Physique Nucléaire Théorique et Physique Mathématique, C.P. 229, Université libre de Bruxelles (ULB), B-1050 Brussels, Belgium

A coupled-channel nucleon-antinucleon interaction model is developed as an alternative to traditional optical models and is adjusted to reproduce the same $N\bar{N}$ low-energy dataset as the Kohno-Weise potential. The scattering lengths of the antiproton-deuteron system and the level shifts of its lowest hydrogenic states are computed by solving the Faddeev-Merkuriev equations in configuration space. The calculations are carried out with two different nucleon-nucleon interactions and the results compared with those obtained with an optical model to explore the model-dependence, which is found to be weak. The antiproton annihilation densities on deuteron are finally calculated and compared.

I. INTRODUCTION

The Low-Energy Antiproton Ring (LEAR) and its rich experimental program at CERN [1–3] have made low-energy antiproton physics an active field of research from the early 1980s until its closure in 1996. More recently, the development of facilities such as the Antiproton Decelerator (AD) or the Extra Low-Energy Antiproton ring (ELENA) has offered new opportunities to study the properties of antimatter, its interplay with standard matter, as well as baryon-antibaryon symmetries through various experiments. Low-energy antiprotons have namely been used for the formation and the study of antiprotonic atoms [1,4]. In these experiments, an antiproton is captured in a highly excited atomic Coulomb orbital, after ejecting one of the electrons. It then decays to lower states by x rays or Auger electron emissions, and finally annihilates with a nucleon under the influence of the strong hadronic interaction. The same mechanism will be exploited in the PUMA experiments [5], which aims to study nucleus skin densities of short-lived isotopes produced by ISOLDE. Low-energy antiproton annihilation is a promising tool to probe the nuclear structure [6–8]. In particular, the measurement of nucleon-antinucleon annihilation products is expected to provide a unique sensitivity to the proton and neutron densities at the surface of the nucleus.

While a qualitative picture of what will happen in the PUMA experiments is known, a fully microscopic treatment of the antiproton-nucleus interaction dynamics remains to be developed. From a theoretical point of view, the description of antiprotonic atoms mainly relies on nucleon-antinucleon ($N\bar{N}$) optical potentials [9–13]. Such models provide a convenient way to include the $N\bar{N}$ annihilation and can be used together with nucleon-nucleon (NN) interactions in *ab initio* calculations. However, the reliability of such approaches is hard to assess due to the limited amount of data available to constrain $N\bar{N}$ interaction models. Since the PUMA project relies on the detection of annihilation products, it is of paramount importance to test the validity of the models which will be used to analyze experimental data. In this paper, an alternative approach to traditionally used optical models is explored, where the annihilation is modeled by the addition of effective meson channels. The coupled-channel potential is adjusted to reproduce the optical model results for $N\bar{N}$ systems, which allows us to investigate the importance of annihilation dynamics in one of the simplest cases of antiproton-nucleus annihilation: the deuteron-antiproton ($d\bar{p}$) system.

If only interacting through the Coulomb interaction, the $d\bar{p}$ spectrum would include an infinite set of well-known Rydberg states, whose energies are approximately provided by

$$E_n^{(C)} = E_B - \frac{R_y(d\bar{p})}{n^2}, \tag{1}$$

where $E_B \approx 2.22$ MeV is the binding energy of the deuteron and $R_y(d\bar{p}) \approx 16.6662$ keV is the $d\bar{p}$ Rydberg energy. Apart QED and relativistic corrections, which these Rydberg states

---

[*]pierre-yves.duerinck@ulb.be
[†]rimantas.lazauskas@iphc.cnrs.fr
[‡]jeremy.dohet-eraly@ulb.be

are affected (these corrections are not considered in this work but can be assessed perturbatively afterwards), they are subject to the strong interaction, which introduces additional shift and broadening (due to finite time it takes to annihilation) of these levels. These atomic states are expected to play an important role in the PUMA experiments. Wave functions and eigenenergies of these states are calculated in this work by solving the Faddeev-Merkuriev equations in configuration space [14,15], employing the coupled-channel approach. The results are then compared with those obtained in Ref. [16], where traditional optical models were considered.

In this paper, the optical and coupled-channel formalisms are first presented. A formal extension of the Faddeev-Merkuriev equation formalism to include particle coupled channels is then presented. The model dependence is investigated by computing and comparing the $d\bar{p}$ scattering lengths obtained with different NN and $N\bar{N}$ models. The complex energy shifts with respect to the energy of the hydrogenic states are then computed from both direct resonant state calculations and from the scattering lengths or volumes by employing the Trueman relation [17]. Finally, the $d\bar{p}$ annihilation is investigated by computing and analyzing the annihilation densities.

II. FORMALISM

A. The $N\bar{N}$ interaction

For a long time the meson-exchange theory was used to formulate the NN interaction [18]. Within this framework, the nuclear interaction is expressed as a sum of different terms, each one associated with the exchange of a specific meson:

$$V_{NN} = \sum_{m=\pi,\rho,\omega,\dots} V_{NN}^{(m)}. \qquad (2)$$

The real part of the $N\bar{N}$ interaction then follows via G-parity transform of the NN interaction [19], providing a multiplicative factor for each term of Eq. (2):

$$U_{N\bar{N}} = \sum_{m=\pi,\rho,\omega,\dots} G^{(m)} V_{NN}^{(m)}, \qquad (3)$$

where $G^{(m)} = \mathcal{C}(-1)^{T_m}$ is the G-parity of the meson m, defined with the charge conjugation operator $\mathcal{C}$ and the meson isospin T_m. To avoid the nonintegrable singularities due to spin-orbit and tensor terms, $U_{N\bar{N}}$ is regularized when the interparticle distance is below a given cutoff radius.

In this work we concentrate on hydrogenic states, which are dominated by $p\bar{p}$ Coulomb interaction, which does not comply to isospin symmetry. Therefore the particle basis involving nucleon-antinucleon pairs is here more appropriate. Using the isospin convention of Ref. [20], the isospin state of the $N\bar{N}$ pairs are given by

$$|p\bar{p}\rangle = \frac{1}{\sqrt{2}}(|0\,0\rangle + |1\,0\rangle), \quad |n\bar{p}\rangle = |1\,-1\rangle,$$

$$|n\bar{n}\rangle = \frac{1}{\sqrt{2}}(|0\,0\rangle - |1\,0\rangle). \qquad (4)$$

The $N\bar{N}$ potential should not only describe the attractive or repulsive features between the particles but should also account for the $N\bar{N}$ annihilation. Given the substantial amount

of energy available in the $N\bar{N}$ annihilation at rest, this process includes a large number of meson-producing channels, mainly involving pions and kaons [21]. This variety of multimeson final states induces complex dynamics presenting a significant challenge to microscopic theories. For this reason, the $N\bar{N}$ annihilation is treated in a phenomenological way. Two different approaches emerge and are hereafter developed: the optical and coupled-channel models.

1. Optical model

In the optical model framework, the annihilation is accounted by the addition of a complex phenomenological term W to $U_{N\bar{N}}$ so that the resulting $N\bar{N}$ potential reads

$$V_{N\bar{N}} = U_{N\bar{N}} + W \quad (W \in \mathbb{C}). \qquad (5)$$

For the sake of numerical convenience, a Woods-Saxon form is often chosen to represent W by fixing the same range and strength parameters for all considered partial waves and adjusting them to fit the experimental data. The imaginary part of the potential induces a loss of probability flux in the $N\bar{N}$ channels, which simulates the cumulative effects of producing mesons. Only the $N\bar{N}$ degrees of freedom are therefore explicitly included in practical calculations. In the present work, we utilize the Kohno-Weise (KW) potential [11], in which W is purely imaginary.

In the particle basis, the coupled-channel Schrödinger equation for $p\bar{p}$, $n\bar{n}$, and $n\bar{p}$ systems can be summarized by

$$\left(E - H_0^{i\bar{j}} - \delta m_{i\bar{j}} c^2\right)\psi_{i\bar{j}} = \sum_{i'\bar{j}'} V_{i\bar{j},i'\bar{j}'}\psi_{i'\bar{j}'}, \qquad (6)$$

where $H_0^{i\bar{j}}$ is the diagonal two-body kinetic-energy operator for a particle-antiparticle pair $i\bar{j}$ and E denotes the energy measured relative to a conventionally chosen threshold $(m_a + m_{\bar{b}})c^2$. Term $\delta m_{i\bar{j}} = m_i + m_{\bar{j}} - m_a - m_{\bar{b}}$ eventually accounts for a mass difference in a coupled-channel case. For the $p\bar{p}$ case, particle indexes span two coupled channels $i\bar{j} = (p\bar{p}, n\bar{n})$, whereas for the $n\bar{p}$ case, the sum is limited to a single channel.

2. Coupled-channel model

In the coupled-channel (CC) approach, the potentials are real $(V_{N\bar{N}} = U_{N\bar{N}})$ and the annihilation is accounted by the addition of effective channels, mimicking the production of the real mesons. In contrast with optical models, where a part of the flux is suppressed by an imaginary potential, the flux is here distributed among the effective channels, providing a unitary S matrix. Within this approach, the annihilation dynamics is more complete, involving the possibility of a nucleon-antinucleon re-emission.

The present model is mainly inspired from Ref. [20]. In that work, to each $N\bar{N}$ channel is associated an effective meson-antimeson $(m\bar{m})$ one coupled by a phenomenological interaction. The properties of these effective particles and the coupling potentials are adjusted for each partial wave to reproduce a selected set of $N\bar{N}$ scattering data. For the sake of simplicity, the effective mesons are supposed to be noninteracting with each other.

Within the CC model, the Schrödinger equation (6) remains formally valid, but more particle-antiparticle channels are involved and thus wave functions contain more components. In particular, for the total charge $Z = 0$ case our model potential couples four particle-antiparticle components and has the following symmetrical structure:

$$\begin{pmatrix} \psi_{m_1 \bar{m}_1} \\ \psi_{m_2 \bar{m}_2} \\ \psi_{p\bar{p}} \\ \psi_{n\bar{n}} \end{pmatrix}, \quad V = \begin{pmatrix} 0 & 0 & V_{p\bar{p},m_1\bar{m}_1} & V_{n\bar{n},m_1\bar{m}_1} \\ 0 & 0 & V_{p\bar{p},m_2\bar{m}_2} & V_{n\bar{n},m_2\bar{m}_2} \\ V_{p\bar{p},m_1\bar{m}_1} & V_{p\bar{p},m_2\bar{m}_2} & V_{p\bar{p},p\bar{p}} & V_{p\bar{p},n\bar{n}} \\ V_{n\bar{n},m_1\bar{m}_1} & V_{n\bar{n},m_2\bar{m}_2} & V_{p\bar{p},n\bar{n}} & V_{n\bar{n},n\bar{n}} \end{pmatrix}. \tag{7}$$

For the $Z = -1$ case, our model is limited to two components:

$$\begin{pmatrix} \psi_{m_3 \bar{m}_3} \\ \psi_{n\bar{p}} \end{pmatrix}, \quad V = \begin{pmatrix} 0 & V_{n\bar{p},m_3\bar{m}_3} \\ V_{n\bar{p},m_3\bar{m}_3} & V_{n\bar{p},n\bar{p}} \end{pmatrix}. \tag{8}$$

For simplicity in studying more complex systems, beyond nucleon-antinucleon case, the mass of the mesons is chosen the same in each channel and partial wave, i.e., $m_{m_1} = m_{m_2} = m_{m_3} = 775.26$ MeV/c^2, which corresponds to the mass of the ρ meson.

Within our CC model, matrix elements coupling $N\bar{N}$ to $N\bar{N}$ channels are based on the meson-exchange potential proposed by Brian and Philipps in Ref. [22] on which the G-parity transform is applied. When the interparticle distance is below the cutoff radius r_c, each isospin component is smoothly extrapolated by imposing a C^1 matching with a polynomial function of degree two. Moreover, isospin symmetry implies that $V_{p\bar{p},p\bar{p}}$ differs from $V_{n\bar{n},n\bar{n}}$ only by the presence of an attractive Coulomb interaction term.

The coupling of $N\bar{N}$ channels with the meson-antimeson ones is realized introducing short-range Yukawa potentials, corresponding to the simplest Feynman diagram for the annihilation process:

$$V_{p\bar{p},m_1\bar{m}_1} = V_{n\bar{n},m_2\bar{m}_2} = \hbar c \lambda_1 r^{-1} e^{-r/r_a}, \tag{9}$$

$$V_{p\bar{p},m_2\bar{m}_2} = V_{n\bar{n},m_1\bar{m}_1} = \hbar c \lambda_2 r^{-1} e^{-r/r_a}, \tag{10}$$

$$V_{n\bar{p},m_3\bar{m}_3} = \hbar c \lambda_3 r^{-1} e^{-r/r_a}, \tag{11}$$

where λ_1, λ_2, λ_3 are the dimensionless amplitudes of the coupling potentials and $r_a = \frac{\hbar c}{m_p} \approx 0.21$ fm is the proton Compton wavelength.

For each partial wave, three parameters need to be adjusted for the $p\bar{p}/n\bar{n}$ system (r_c, λ_1, and λ_2) and two parameters for the $n\bar{p}$ system (r_c, λ_3). For coupled waves, an additional cutoff radius is introduced to extrapolate the transition tensor potential at short distances. To investigate the model dependence and the effects of annihilation dynamics in a three-body system, the parameters of the coupled-channel potential are adjusted to fit the low-energy S matrix provided by the KW model. The fitting procedure consists in a simple least-square fit of the S-matrix elements for $N\bar{N}$ energies ranging from $E = 0$ to 12 MeV in the center of mass frame, and has been realized for partial waves with $l \leqslant 5$. The parameters for the $p\bar{p}$ and $n\bar{p}$ systems are given in the Appendix. Some of the $p\bar{p}$ and $n\bar{p}$ scattering lengths computed with the coupled-channel and Kohno-Weise models are given in Table I for comparison. The $N\bar{p}$ scattering lengths are reproduced with

TABLE I. $N\bar{p}$ scattering lengths and volumes computed with the KW and CC models.

$^{2S+1}L_J$	$p\bar{p}$ (KW)	$p\bar{p}$ (CC)	$n\bar{p}$ (KW)	$n\bar{p}$ (CC)
	a_0 (fm)	a_0 (fm)	a_0 (fm)	a_0 (fm)
$^1S_0$	$0.57 - 0.77$i	$0.57 - 0.76$i	$1.07 - 0.62$i	1.07–0.61 i
$^3SD_1$	$0.92 - 0.63$i	$0.90 - 0.65$i	$0.78 - 0.80$i	0.78–0.79 i
	a_1 (fm^3)	a_1 (fm^3)	a_1 (fm^3)	a_1 (fm^3)
$^1P_1$	$-1.19 - 0.53$i	$-1.12 - 0.54$i	$0.71 - 0.47$i	$0.70 - 0.49$i
$^3P_0$	$-2.77 - 1.99$i	$-2.82 - 1.84$i	$2.43 - 0.11$i	$2.39 - 0.11$i
$^3P_1$	$1.22 - 0.47$i	$1.19 - 0.48$i	$-2.17 - 0.95$i	$-2.07 - 0.98$i
$^3PF_2$	$-0.36 - 0.75$i	$-0.32 - 0.73$i	$-0.30 - 0.45$i	$-0.29 - 0.47$i

5% accuracy or better. The calculations have been carried out with the nucleon masses $m_p = 938.2721$ MeV/c^2 and $m_n = 939.5654$ MeV/c^2.

B. Faddeev-Merkuriev equations

The deuteron-antiproton ($d\bar{p}$) system consists of two coupled three-particle bases ($p, n, \bar{p}$) and ($n, n, \bar{n}$), when optical $N\bar{N}$ interaction models are considered. The coupled-channel model generates additional three-particle bases, associated with the dynamical production of meson-antimeson pairs (as will be detailed in what follows). The Faddeev equation's ansatz is based on splitting systems wave function into Faddeev components (FCs) associated with each possible combination of $(2 + 1)$-particle clusters.

It is convenient to express these components by associating a Jacobi coordinate set to each of them:

$$\boldsymbol{x}_i = \sqrt{\frac{2m_j m_k}{m_0(m_j + m_k)}} (\boldsymbol{r}_k - \boldsymbol{r}_j), \tag{12}$$

$$\boldsymbol{y}_i = \sqrt{\frac{2m_i(m_j + m_k)}{m_0(m_i + m_j + m_k)}} \left(\boldsymbol{r}_i - \frac{m_j \boldsymbol{r}_j + m_k \boldsymbol{r}_k}{m_j + m_k} \right), \tag{13}$$

where (i, j, k) is a cyclic permutation of (1,2,3), $\boldsymbol{r}_i$ is the position of particle i, m_i its mass, and m_0 a reference mass chosen arbitrarily for the coherence of the units.

1. Optical model

Using $N\bar{N}$ optical models there are six different FCs associated with the following particle configurations:

$$(np)\bar{p}, \quad (\bar{p}n)p, \quad (p\bar{p})n, \quad (nn)\bar{n}, \quad (\bar{n}n)n, \quad (n\bar{n})n. \tag{14}$$

The last two components are formally identical; the wave function is antisymmetric relative to the permutation of two neutrons so that the last component can be comfortably written in terms of the fifth one.

The remaining five components are related by the following Faddeev-type equations:

$$\left(E - H_0^{ijk} - \delta m_{ijk} c^2 \right) \Psi_{ij,k}$$
$$= \sum_{i'j'} V_{ij,i'j'} (\Psi_{i'j',k} + \Psi_{ki',j'} + \Psi_{j'k,i'}). \tag{15}$$

These equations enable in theory to study deep bound states in $NN\bar{N}$ systems. However they are not appropriate numerically to study $d\bar{p}$ Rydberg states and low-energy antiproton scattering on deuteron, which are dominated by the long-ranged Coulomb attraction between proton and antiproton. The former equations were modified as proposed by Merkuriev, in order to separate $d\bar{p}$ Coulomb asymptote in a single Faddeev-Merkuriev component (FMC), namely $\Psi_{np,\bar{p}}$. This feature is realized by splitting, attractive $p\bar{p}$ Coulomb interaction into long-ranged and short-ranged parts:

$$V_{C,p\bar{p}}(x_{p\bar{p}}) = V_C^l(x_{p\bar{p}}, y_{p\bar{p},n}) + V_C^s(x_{p\bar{p}}, y_{p\bar{p},n}), \qquad (16)$$

as explained in Ref. [15]. Equation (15) is then modified as

$$\left(E - H_0^{ijk} - \delta m_{ijk}c^2 - V_{C,ik}^l - V_{C,jk}^l\right)\Psi_{ij,k}$$
$$= \sum_{i'j'} V_{ij,i'j'}(\Psi_{i'j',k} + \Psi_{ki',j} + \Psi_{j'k,i'})$$
$$- V_{C,ij}^l(\Psi_{ki,j} + \Psi_{jk,i}). \qquad (17)$$

2. Coupled-channel model

The coupled-channel approach introduces explicitly new particle channels related with production of $m_1\bar{m}_1$, $m_2\bar{m}_2$, and $m_3\bar{m}_3$ meson pairs. Therefore the $d\bar{p}$ system involves five three-particle combinations, namely: $(p\bar{p}n)$, $(n\bar{n}n)$, $(m_1\bar{m}_1n)$, $(m_2\bar{m}_2n)$, $(m_3\bar{m}_3p)$. The wave function formally includes 15 FMCs and satisfies similar Faddeev-Merkuriev equations set to Eq. (17).

Nevertheless, as our model supposes that mesons m_1, m_2, and m_3 do not interact with each other nor with nucleons, apart annihilation, all the FMCs associated with a spectator (anti)meson turn to be null:

$$\Psi_{m_iN,\bar{m}_i} \equiv \Psi_{N\bar{m}_i,m_i} \equiv 0. \qquad (18)$$

This leaves us with nine nontrivial FMCs for which system of equations (17) should be solved. These components are associated with the following $2 + 1$ particle clusters:

$$(np)\bar{p}, \quad (\bar{p}n)p, \quad (p\bar{p})n, \quad (nn)\bar{n}, \quad (\bar{n}n)n,$$
$$(m_1\bar{m}_1)n, \quad (m_2\bar{m}_2)n, \quad (m_3\bar{m}_3)p. \qquad (19)$$

Unlike in optical models, the $d\bar{p}$ Rydberg states in the CC model are resonances which cannot be described by square-integrable wave functions. The wave function, describing these states, should include components dynamically describing conversion into stable nucleon-meson-antimeson configurations. Nevertheless employing complex-scaling (CS) method, the divergent resonant states are transformed into square-integrable functions [23,24]. By the mean of the complex scaling operator $U(\theta)$, the three-body wave function and Hamiltonian are transformed into

$$\Psi^\theta(\boldsymbol{x}, \boldsymbol{y}) = U(\theta)\Psi(\boldsymbol{x}, \boldsymbol{y}) = e^{3i\theta}\Psi(\boldsymbol{x}e^{i\theta}, \boldsymbol{y}e^{i\theta}), \qquad (20)$$

$$H^\theta = U(\theta)HU^{-1}(\theta), \qquad (21)$$

satisfying

$$H^\theta\Psi^\theta = E^\theta\Psi^\theta. \qquad (22)$$

Furthermore, as the production of nucleon-meson-antimeson components generates an important amount of kinetic energy,

after CS transformation even with relatively small angles these components decrease fast.

3. Numerical resolution

For both models, the Faddeev-Merkuriev equations are solved numerically for states defined by a total angular momentum J and parity π by expanding each FMC in a partial-wave expansion:

$$\Psi_i^\theta(\boldsymbol{x}_i, \boldsymbol{y}_i) = \sum_n \frac{\phi_n^{(\theta,i)}(x_i, y_i)}{x_i y_i} \mathcal{Y}_n(\hat{x}_i, \hat{y}_i), \qquad (23)$$

where the index n includes the orbital momenta and spins (l_x, l_y, L, s_x, S), $\phi_n^{(\theta,i)}$ is a radial function to be computed, and $\mathcal{Y}_n(\hat{x}_i, \hat{y}_i)$ is a bipolar spherical harmonics including the coupling of orbital momenta and spins. When optical potentials are considered, $\theta = 0$ is chosen. Once projected onto an amplitude $\mathcal{Y}_n$, the radial Faddeev-Merkuriev equations are obtained as

$$\sum_{n'} \mathcal{D}_{nn'}\phi_{n'}^{(\theta,i)}(x_i, y_i) = \sum_{n'n''} V_{nn'}(x_ie^{i\theta}, y_ie^{i\theta})$$
$$\times \int_{-1}^1 h_{n'n''}(x_i, y_i, u)\phi_{n''}^{(\theta,j)}(x_j, y_j)\mathrm{d}u, \qquad (24)$$

where $h_{n'n''}$ is some integral kernel and $\mathcal{D}_{nn'}$ is the differential operator defined as

$$\mathcal{D}_{nn'} = E^\theta\delta_{nn'} + e^{-2i\theta}\left[\frac{\hbar^2}{m_0}\frac{\partial^2}{\partial x_i^2} + \frac{\hbar^2}{m_0}\frac{\partial^2}{\partial y_i^2} - \frac{\hbar^2}{m_0}\frac{l_{x_n}(l_{x_n}+1)}{x_i^2}\right.$$
$$\left. - \frac{\hbar^2}{m_0}\frac{l_{y_n}(l_{y_n}+1)}{y_i^2}\right]\delta_{nn'} - V_{nn'}(x_ie^{i\theta}, y_ie^{i\theta}). \qquad (25)$$

The radial functions are expressed on a two-dimensional regularized Lagrange-Laguerre mesh with

$$\phi_n^{(\theta,i)}(x_i, y_i) = \sum_{\alpha=1}^{k_x}\sum_{\beta=1}^{k_y} c_{n\alpha\beta}^{(\theta,i)}\hat{f}_\alpha\left(\frac{x_i}{h_x}\right)\hat{f}_\beta\left(\frac{y_i}{h_y}\right), \qquad (26)$$

with $\hat{f}_i(r)$ a Lagrange-Laguerre function regularized by $\sqrt{r}$ [25]. The use of such basis makes particularly simple the computation of the radial matrix elements with a Gauss-Laguerre quadrature. The scaling parameters h_x and h_y are chosen to adjust the grid size to the considered system. The mesh points distribution for the x coordinate is mainly governed by the deuteron wave function. The motion in y should account for both nuclear and long-range interactions between the antiproton and deuteron, which requires a larger spatial extension. When projecting Faddeev-Merkuriev equations onto the basis of Eq. (26), the differential equations are converted into a system of linear equations. Its resolution provides the coefficients required to evaluate the complex-scaled wave function Ψ^θ which is used in this work to compute the annihilation densities. The wave function Ψ can be extracted by considering the direct back-rotation:

$$\Psi(\boldsymbol{x}, \boldsymbol{y}) = e^{-3i\theta}\Psi^\theta(\boldsymbol{x}e^{-i\theta}, \boldsymbol{y}e^{-i\theta}), \qquad (27)$$

but it turns out to be a mathematically ill-defined problem [26]. If applied directly this causes severe numerical instabilities, due to introduction of high-frequency noise in back-rotated wave functions. In practice this approach provides numerically stable results only for the wave function region around the origin and only when small values of θ are involved. A stabilization method has been proposed in Ref. [27] and is based on the Tikhonov regularization of the rotated wave function Fourier transform. It is shown that the radial wave function of Faddeev amplitude n reads

$$
\phi_n^{(\theta,i)}(xe^{-i\theta}, ye^{-i\theta}) = \int_0^\infty \int_0^\infty F(u', u, \theta, \kappa_x) F(v', v, \theta, \kappa_y)
$$
$$
\times \; \phi_n^{(\theta,i)}(x_0 e^{-u'}, y_0 e^{-v'}) \mathrm{d}u' \mathrm{d}v', \quad (28)
$$

where $u = -\ln(x/x_0)$, $v = -\ln(y/y_0)$, x_0, and y_0 are length parameters selected here at $x_0 = y_0 = 1$ fm, and κ_x and κ_y are smoothing parameters for each coordinate. The function F is defined as

$$
F(u', u, \theta, \kappa) = \frac{{}_2F_1\left(1, \frac{i(u-u')}{2\theta} + \frac{1}{2}; \frac{i(u-u')}{2\theta} + \frac{3}{2}; -\frac{1}{\kappa}\right)}{\kappa(iu - iu' + \theta)}
$$
$$
+ \frac{{}_2F_1\left(1, \frac{1}{2} - \frac{i(u-u')}{2\theta}; \frac{3}{2} - \frac{i(u-u')}{2\theta}; -\kappa\right)}{-iu + iu' + \theta}, \quad (29)
$$

where ${}_2F_1$ is a hypergeometric function.

In our calculations, the following constants have been used: $\hbar c = 197.32698$ MeV fm, the fine-structure constant $\alpha = 1/137.0360$, and $\hbar^2/m_N = 41.4711$ MeV fm^2 where m_N is the nucleon mass. The partial-wave expansion of each Faddeev component includes all amplitudes with $l_x + l_y \leqslant 8$.

III. RESULTS

The purpose of this paper is to investigate the model dependence in the description of the $d\bar{p}$ three-body states by comparing the results obtained with the KW and CC models, which involve very different annihilation dynamics. Even though the $d\bar{p}$ orbital momentum is not a good quantum number since it is not conserved by the nuclear interaction, it remains relevant for describing $d\bar{p}$ atomic states, which extend far beyond the range of nuclear forces. In the following, the partial waves under study are therefore denoted with the spectroscopic notation L_J^π, where L is the orbital momentum between the deuteron and the antiproton.

A. Scattering lengths

By imposing the appropriate asymptotic behavior for the $\Psi_{np,\bar{p}}$ component, the zero-energy $d\bar{p}$ collision has first been studied. Within the CC approach, the scattering lengths and wave functions have been computed by using the complex-scaling method with θ values of a few degrees. The results are given in Table II and compared with those obtained with the KW model. Two NN interactions have been considered for the calculations: the central Malfliet-Tjon potential [28] and the realistic Argonne V18 potential [29], allowing us to investigate the importance of the deuteron SD coupling in the three-body problem. When compared with the KW model, the convergence and the stability for the CC model with respect

TABLE II. $d\bar{p}$ scattering lengths computed with different $NN + N\bar{N}$ interactions.

L_J^π	MT + KW [16]	MT + CC	AV18 + KW [16]	AV18 + CC
	a_0 (fm)	a_0 (fm)	a_0 (fm)	a_0 (fm)
$S_{1/2}^+$	1.341 − 0.717i	1.32 − 0.71i	1.335 − 0.716i	1.32 − 0.68i
$S_{3/2}^+$	1.394 − 0.724i	1.40 − 0.73i	1.385 − 0.721i	1.39 − 0.74i
	a_1 (fm^3)	a_1 (fm^3)	a_1 (fm^3)	a_1 (fm^3)
$P_{5/2}^-$	0.714 − 2.64i	0.6 − 2.7i	0.699 − 2.61i	0.6 − 2.6i

to the grid parameters is slightly worse, requiring a larger number of radial functions ($k_x \approx 40$–50, $k_y \approx 50$–70). The scaling parameters h_x and h_y have been chosen between 0.2 fm and 0.3 fm. The accuracy is given within three digits, with an uncertainty of few units for the last one.

Results in Table II prove to be rather independent on the NN interaction model in use. It is the case, at least, for asymptotically spin-uncoupled partial waves. As stated in Ref. [16], energy shifts of asymptotically coupled spin-angular-momentum states might depend more strongly on deuteron properties and in particular on its quadrupole moment.

Despite their very different implementation of the $N\bar{N}$ annihilation, the KW and the CC models provide close values for both the real and the imaginary part of scattering lengths, with relative differences of few percent. This difference is compatible with discrepancy reproducing low-energy $N\bar{N}$ data. The smallest differences appear for the S waves. This agreement could indicate the small impact of the off-energy shell effects on three-body dynamics at low energies and probably smaller importance of three-body forces, relative to one observed in three-nucleon (which account for $\approx 10\%$ effect in calculated binding energies). This also hints on potential predictivity of $N\bar{N}$ interaction models in describing more complex systems.

B. Level shifts and Trueman relation

Due to the $N\bar{N}$ annihilation, the energy E_n of $d\bar{p}$ states includes a negative imaginary part reflecting the finite lifetime of the antiprotonic states:

$$
E_n = E_R - i\frac{\Gamma}{2}. \quad (30)
$$

The shift introduced by the nuclear forces with respect to the energy of the Rydberg states is defined as

$$
\Delta E_n = E_n - E_n^{(C)} = \Delta E_R - i\frac{\Gamma}{2}, \quad (31)
$$

and can be calculated by computing the eigenvalues of a complex Hamiltonian. Its complex nature arises either from the potential for optical models or from the complex scaling within the coupled-channel approach. In both cases, the grid extension has to be adjusted to the size of the hydrogenic states but should also capture the effects of short-range nuclear forces. These requirements are fulfilled by considering a standard Lagrange-Laguerre mesh with a large number of

TABLE III. $d\bar{p}$ energy shifts obtained from the direct calculation (ΔE_n) and from the Trueman relation ($\Delta E^{(T)}$) for different $NN + N\bar{N}$ interactions.

L_J^π	MT + KW [16]		MT + CC	
	ΔE_n (keV)	$\Delta E_n^{(T)}$ (keV)	ΔE_n (keV)	$\Delta E_n^{(T)}$ (keV)
$S_{1/2}^+$ ($n = 1$)	$1.922 - 0.887i$	$1.925 - 0.890i$	$1.91 - 0.86i$	$1.90 - 0.88i$
$S_{3/2}^+$ ($n = 1$)	$2.000 - 0.891i$	$1.991 - 0.880i$	$1.99 - 0.89i$	$1.99 - 0.90i$
	ΔE_n (meV)	$\Delta E_n^{(T)}$ (meV)	ΔE_n (meV)	$\Delta E_n^{(T)}$ (meV)
$P_{5/2}^-$ ($n = 2$)	$51.8 - 213i$	$55.4 - 205i$		$46.5 - 209i$
	AV18 + KW [16]		AV18 + CC	
	ΔE_n (keV)	$\Delta E_n^{(T)}$ (keV)	ΔE_n (keV)	$\Delta E_n^{(T)}$ (keV)
$S_{1/2}^+$ ($n = 1$)	$1.913 - 0.886i$	$1.917 - 0.890i$	$1.87 - 0.86i$	$1.88 - 0.85i$
$S_{3/2}^+$ ($n = 1$)	$1.987 - 0.889i$	$1.979 - 0.888i$	$1.84 - 0.95i$	$1.98 - 0.91i$
	ΔE_n (meV)	$\Delta E_n^{(T)}$ (meV)	ΔE_n (meV)	$\Delta E_n^{(T)}$ (meV)
$P_{5/2}^-$ ($n = 2$)	$61.2 - 207i$	$54.2 - 202i$		$46.5 - 201i$

points or more efficiently with a combination of Lagrange-Legendre and Lagrange-Laguerre meshes as in Ref. [16].

The complex level shifts can also be approximately computed from the scattering length a_l by employing the Trueman relation [17]. Initially formulated for S and P waves, the generalized Trueman formula takes the form of the following expansion:

$$\frac{\Delta E_n}{\epsilon_n} = -\frac{4}{n} \frac{a_l}{B^{2l+1}} \alpha_{n,l} \left(1 - \frac{a_l}{B^{2l+1}} \beta_{n,l} \right), \qquad (32)$$

where B is the $d\bar{p}$ Bohr radius, and $\alpha_{n,l}$ and $\beta_{n,l}$ are some numerical coefficients defined in Ref. [30]. It has been already shown in Ref. [30] that the Trueman relation is very accurate for atomic states of protonium and is consistent with the direct calculation of the Hamiltonian eigenvalues for $d\bar{p}$ states described with the KW model [16].

Table III contains the complex energy shifts for the same models and partial waves as Table II. The column ΔE_n represents the value obtained from the direct $d\bar{p}$ resonant state calculations while $\Delta E^{(T)}$ is the energy shift obtained from the Trueman relation and the scattering lengths listed in Table II. For all models, the use of the Trueman relation is consistent with the direct calculations, especially for S waves. Concerning the P wave, a fair agreement is also observed with the KW potential. However, the value ΔE_n could not be computed when applying the complex-scaling method: since the P-wave energy shift is six orders of magnitude smaller than for the S-wave ones, the small energy dependence in θ introduced by the complex scaling turns out to be of the same order of magnitude as the energy shift induced by the strong interactions. The value obtained from the Trueman relation is however quite close to the one of the KW model, which confirms the observed model independence. Calculation of the scattering length is an easier task than the resonant state one, due to considerably smaller grid sizes required to accomplish these calculations. Indeed, they are determined by the size of the deuteron and the range of the nuclear potential, which are much smaller than extensions of the Rydberg states. This indirect approaches appears as a promising alternative for the description of the Rydberg energy shifts in heavier nuclei.

Nevertheless, we should point out that it is yet limited to spin-uncoupled partial waves in the asymptote such as $S_{1/2}^+$, $S_{3/2}^+$, and $P_{5/2}^-$ ones. Since the deuteron is not spherically symmetric, the asymptotic deuteron-antiproton interaction includes, in addition to the Coulomb potential in $1/r$, other multipole terms starting with the quadrupole one in $1/r^3$. Due to these additional contributions, several partial waves such as $P_{1/2}^-$ or $P_{3/2}^-$ are asymptotically coupled for which the modified Coulomb effective range expansion and the Trueman relation are not valid anymore.

C. Annihilation densities

From the three-body wave function, the resonance width Γ can be obtained by computing the expectation value of the Hamiltonian:

$$\Gamma = -2\mathrm{Im}[\langle \Psi_{d\bar{p}} | H | \Psi_{d\bar{p}} \rangle], \qquad (33)$$

where $\Psi_{d\bar{p}} = \Psi_{np,\bar{p}} + \Psi_{p\bar{p},n} + \Psi_{\bar{p}n,p}$. Equation (33) can be expressed as a unidimensional integral:

$$\Gamma = \int_0^\infty \gamma_a(y) \mathrm{d}y, \qquad (34)$$

where γ_a is the annihilation density defined by

$$\gamma_a(y) = -2\mathrm{Im}\left\{ \int \Psi_{d\bar{p}}^*(\mathbf{x}, \mathbf{y})[E - H_0]\Psi_{d\bar{p}}(\mathbf{x}, \mathbf{y})\mathrm{d}\mathbf{x}\mathrm{d}\hat{\mathbf{y}} \right\} \qquad (35)$$

and is usually interpreted as the annihilation probability with respect to the distance y between the antiproton and the deuteron center of mass. A similar definition exists for two-body systems [20]. The PUMA project is based on the intuitive idea that the annihilation is more likely to happen in the periphery of the nucleus. The consistency of this hypothesis can be verified by comparing the $d\bar{p}$ annihilation densities to the nuclear density of deuteron. The annihilation densities are here computed on the basis of the zero-energy scattering wave functions, which are expected to be very similar to the hydrogenic ones in the region governed by the nuclear interaction. The deuteron nuclear density is scaled appropriately for the comparison.
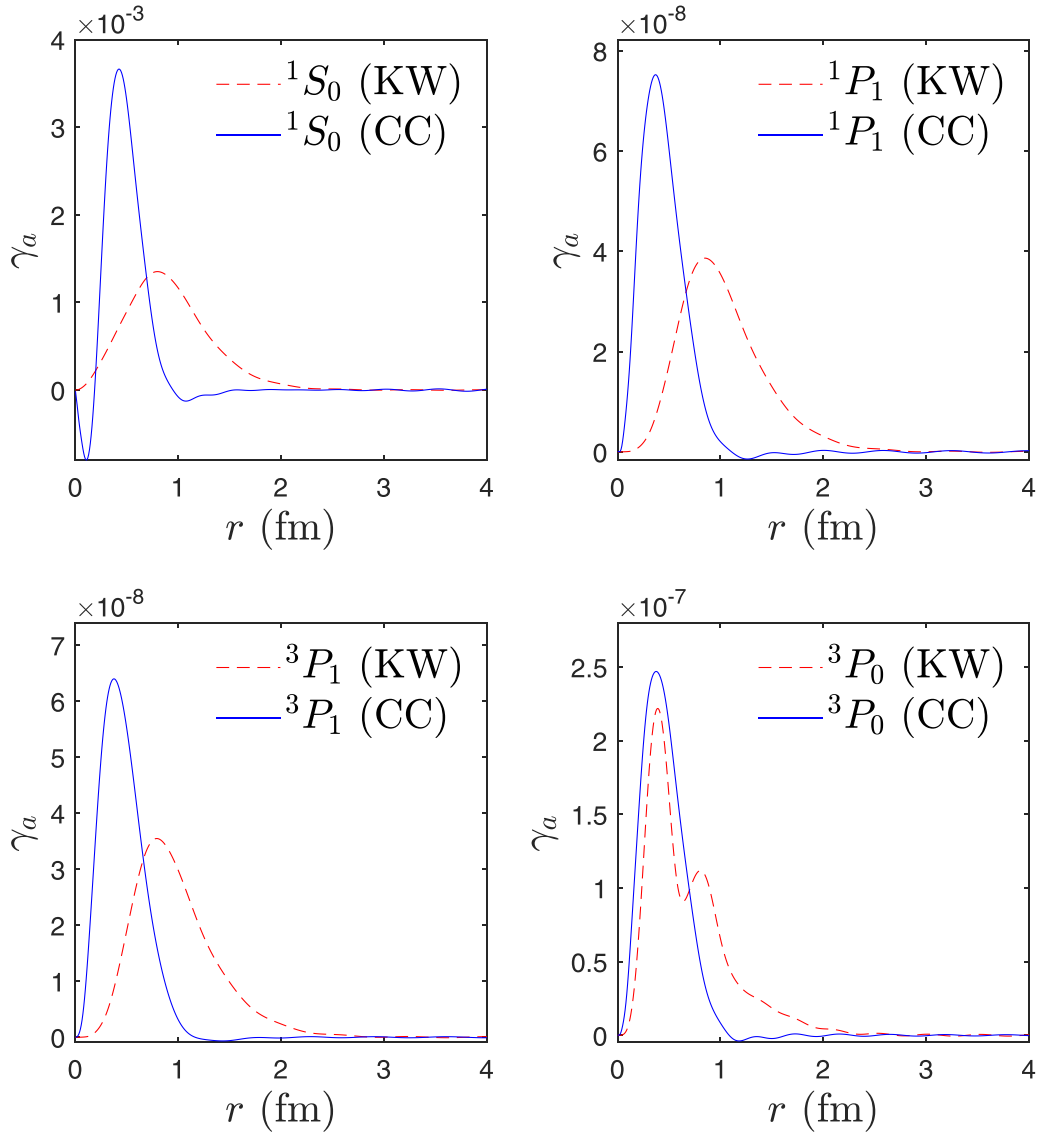
FIG. 1. S- and P-wave $p\bar{p}$ annihilation density computed with the KW (red dashed line) and CC (blue full line) models

The $N\bar{N}$ annihilation densities have already been extensively studied with traditional optical potentials [31–33]. Expectedly, in these works, significant differences were observed among the considered models. Indeed, several Hamiltonian corresponding with nearly identical observables quantities, may lead to dramatically different annihilation densities inside the interaction region. Given the very different background of optical and coupled-channel models, similar conclusions are therefore expected. The $p\bar{p}$ annihilation densities computed with the KW and CC models illustrate well the difference in terms of annihilation dynamics, as it can be observed in Fig. 1. While the $^1S_0$ KW annihilation density includes a broad peak centered at $r \approx 0.8$ fm and is always positive, the CC one includes a narrower peak centered at $r \approx 0.42$ fm and is negative in some regions. With the optical model, flux is only suppressed from the $p\bar{p}$ channel to model the annihilation ($W < 0$), resulting in a positive function. With the coupled-channel model, the situation is more complex and the exchange of flux between the $p\bar{p}$ and

$m\bar{m}$ channels may locally introduce negative parts to the annihilation density. Moreover, while the KW model strongly suppresses the wave function close to the origin, it is not the case within the coupled-channel approach where high-energy channels are involved, resulting in a more complex structure at short distances. Concerning P waves, the annihilation densities computed with the CC models present a peak which is narrower and slightly shifted closer to the origin in comparison to those computed with the KW model. The $d\bar{p}$ annihilation densities computed with the MT + KW and MT + CC models are shown in Fig. 2 for S (left panel) and P waves (right panel). While the two-body annihilation densities are very different, the curves of Fig. 2 are much more look-alike, which highlights the fact that antiprotons are not very likely to penetrate well inside the nucleus. For the S wave, the peak of the CC density is slightly shifted relative to the KW result. With both models, the S-wave annihilation density decreases faster than the deuteron density, which means that the antiproton is still able to penetrate into the nucleus before
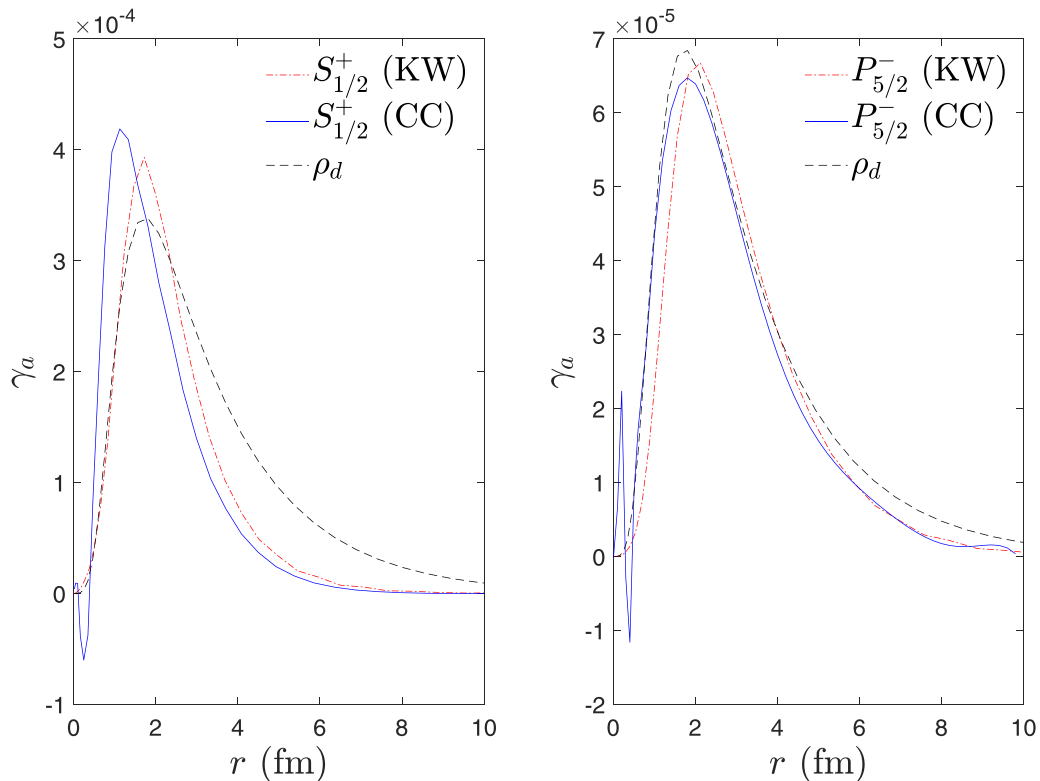
FIG. 2. $S_{1/2}^+$ (left) and $P_{5/2}^-$ (right) $d\bar{p}$ annihilation densities computed with the MT + KW (red dash-doted line) and MT + CC models (blue full line). These curves are compared with the appropriately scaled deuteron density (black dashed line).

being annihilated. The *P*-wave annihilation densities are more similar. Moreover, the asymptotes of the curves scale closely to the deuteron density, with a similar exponential decay pattern. The sensitivity to the tail of nuclear density indicates a peripheral annihilation, which tends to confirm PUMA's main hypothesis.

IV. CONCLUSION

We have considered an alternative approach to optical models, based on the addition of effective meson channels for describing the $N\bar{N}$ annihilation. The parameters of the coupled-channel models have been adjusted to fit the low-energy *S* matrix obtained with the KW model for $p\bar{p}$, $n\bar{n}$, and $n\bar{p}$ systems. The antiproton-deuteron states have then been computed by solving the Faddeev-Merkuriev equations with both optical and coupled-channel models to test the model dependence relative to the $N\bar{N}$ input. The influence of the NN interaction has also been discussed.

Despite their very different dynamics, the $d\bar{p}$ scattering lengths and resonance energies computed with the CC and KW models are fairly similar. The use of the coupled-channel potential is however more tedious due to the additional Faddeev components and the three-body breakup in meson channels, and involves a slower convergence in comparison to its optical counterpart. The calculation of the complex energy shifts with the Trueman relation provides consistent results relative to the bound-state calculations, while requiring less numerical effort. This indirect approach is therefore

promising for heavier nuclei. A generalization of this method to spin-coupled partial waves is however yet to be developed.

In PUMA's experiments, the annihilation is assumed to happen far from the nucleus center. To test the consistency of this hypothesis, we computed the $d\bar{p}$ annihilation densities and compared them with the deuteron nuclear density. For *S* wave, the CC and KW curves are sightly shifted with respect to each other and decrease faster than the nuclear density. A significant fraction of the annihilation is nevertheless expected to happen far from the deuteron center. The sensitivity to the nuclear density tail is more visible for *P* waves where the annihilation densities are more similar and follow more closely the asymptote of the deuteron density, which indicates the dominance of the peripheral absorption of the antiprotons.

TABLE IV. Parameters of the $p\bar{p}$ coupled-channel potential adjusted to fit the low-energy S-matrix obtained with the Kohno-Weise potential.

$^{2S+1}L_J$	r_c (fm)	λ_1	λ_2
$^1S_0$	0.995	12.043	4.417
$^3P_0$	1.368	8.764	-0.5860
$^1P_1$	1.083	8.705	0.039
$^3P_1$	1.173	13.568	4.902
$^3S_1$	2.182	2.237	-4.926
$^3D_1$	0.956	11.280	-9.500
$^3SD_1$	0.789		
$^1D_2$	1.201	22.475	-0.145
$^3D_2$	1.310	11.355	-11.355
$^3P_2$	1.163	8.679	-0.1485
$^3F_2$	1.796	-3.567	0.0325
$^3PF_2$	1.346		
$^1F_3$	0.350	11.395	-8.955
$^3F_3$	1.972	1.039	-0.4280
$^3D_3$	1.512	8.3445	14.576
$^3G_3$	1.290	-3.012	-0.187
$^3DG_3$	1.336		
$^1G_4$	0.300	31.00	0.0
$^3G_4$	2.155	4.685	-0.170
$^3F_4$	0.930	0.386	4.156
$^3H_4$	0.616	-4.877	2.371
$^3FH_4$	0.877		

TABLE V. Parameters of the $n\bar{p}$ coupled-channel potential adjusted to fit the low-energy S-matrix obtained with the Kohno-Weise potential.

$^{2S+1}L_J$	r_c (fm)	λ_3
$^1S_0$	0.910	2.063
$^3P_0$	0.854	7.619
$^1P_1$	1.134	8.710
$^3P_1$	1.178	8.698
$^3S_1$	0.967	7.545
$^3D_1$	0.459	9.257
$^3SD_1$	1.479	
$^1D_2$	1.396	22.926
$^3D_2$	0.467	6.287
$^3P_2$	1.396	8.748
$^3F_2$	0.629	7.538
$^3PF_2$	0.699	
$^1F_3$	3.170	0.810
$^3F_3$	0.523	21.43
$^3D_3$	1.172	22.64
$^3G_3$	0.694	3.811
$^3DG_3$	1.814	
$^1G_4$	3.170	7.042
$^3G_4$	0.319	23.35
$^3F_4$	0.710	1.129
$^3H_4$	0.432	4.240
$^3FH_4$	0.677	

made by GENCI (Grand Equipement National de Calcul Intensif).

APPENDIX: COUPLED-CHANNEL POTENTIAL PARAMETERS

The parameters of the coupled-channel potential adjusted to fit the low-energy S matrix computed with the KW model are collected in Tables IV and V for $p\bar{p}$ and $n\bar{p}$ systems. The first column represents the cutoff radius for the $N\bar{N}$ potential close to the origin while the others represent the dimensionless amplitudes of the Yukawa potentials coupling the meson channels to the $N\bar{N}$ ones.

[1] C. J. Batty, Rep. Prog. Phys. **52**, 1165 (1989).

[2] M. Augsburger, D. Anagnostopoulos, G. Borchert, D. Chatellard, J.-P. Egger, P. El-Khoury, H. Gorke, D. Gotta, P. Hauser, P. Indelicato, K. Kirch, S. Lenz, K. Rashid, T. Siems, and L. M. Simons, Nucl. Phys. A **658**, 149 (1999).

[3] D. Gotta, Prog. Part. Nucl. Phys. **52**, 133 (2004).

[4] T. Yamazaki, N. Morita, R. S. Hayano, E. Widmann, and J. Eades, Phys. Rep. **366**, 183 (2002).

[5] T. Aumann, W. Bartmann, O. Boine-Frankenheim, A. Bouvard, A. Broche, F. Butin, D. Calvet, J. Carbonell, P. Chiggiato, H. De Gersem, R. De Oliveira, T. Dobers, F. Ehm, J. F. Somoza, J. Fischer, M. Fraser, E. Friedrich, A. Frotscher, M. Gomez-Ramos, J.-L. Grenard et al., Eur. Phys. J. A **58**, 88 (2022).

[6] J. Eades and F. J. Hartmann, Rev. Mod. Phys. **71**, 373 (1999).

[7] A. Trzcińska, J. Jastrzębski, P. Lubiński, F. J. Hartmann, R. Schmidt, T. von Egidy, and B. Kłos, Phys. Rev. Lett. **87**, 082501 (2001).

[8] B. Kłos, A. Trzcińska, J. Jastrzębski, T. Czosnyka, M. Kisieliński, P. Lubiński, P. Napiorkowski, L. Pieńkowski, F. J. Hartmann, B. Ketzer, P. Ring, R. Schmidt, T. von Egidy, R. Smolańczuk, S. Wycech, K. Gulda, W. Kurcewicz, E. Widmann, and B. A. Brown, Phys. Rev. C **76**, 014311 (2007).

[9] C. B. Dover and J.-M. Richard, Phys. Rev. C **21**, 1466 (1980).

[10] J. Côté, M. Lacombe, B. Loiseau, B. Moussallam, and R. Vinh Mau, Phys. Rev. Lett. **48**, 1319 (1982).

[11] M. Kohno and W. Weise, Nucl. Phys. A **454**, 429 (1986).

[12] B. El-Bennich, M. Lacombe, B. Loiseau, and S. Wycech, Phys. Rev. C **79**, 054001 (2009).

[13] L.-Y. Dai, J. Haidenbauer, and U.-G. Meißner, J. High Energy Phys. (online) 07 (2017) 078.

[14] L. D. Faddeev, Zh. Eksp. Teor. Fiz. **39**, 1459 (1960) [Sov. Phys. JETP **12**, 1014 (1961)].

[15] S. Merkuriev, Ann. Phys. (NY) **130**, 395 (1980).

[16] R. Lazauskas and J. Carbonell, Phys. Lett. B **820**, 136573 (2021); P.-Y. Duerinck, R. Lazauskas, and J. Carbonell, ibid. **841**, 137936 (2023).

[17] T. Trueman, Nucl. Phys. **26**, 57 (1961).

[18] T. A. Rijken, M. M. Nagels, and Y. Yamamoto, Prog. Theor. Phys. Suppl. **185**, 14 (2010).

[19] C. B. Dover, Nucl. Phys. A **416**, 313 (1984).

[20] E. Ydrefors and J. Carbonell, Eur. Phys. J. A **57**, 303 (2021).

[21] C. B. Dover, T. Gutsche, M. Maruyama, and A. Faessler, Prog. Part. Nucl. Phys. **29**, 87 (1992).

[22] R. A. Bryan and R. J. N. Phillips, Nucl. Phys. B **5**, 201 (1968).

[23] T. Myo and K. Kato, Prog. Theor. Exp. Phys. **2020**, 12A101 (2020).

[24] R. Lazauskas, Few-Body Syst. **54**, 717 (2013).

[25] D. Baye, Phys. Rep. **565**, 1 (2015).

[26] A. Csótó, B. Gyarmati, A. T. Kruppa, K. F. Pál, and N. Moiseyev, Phys. Rev. A **41**, 3469 (1990).

[27] A. T. Kruppa, G. Papadimitriou, W. Nazarewicz, and N. Michel, Phys. Rev. C **89**, 014330 (2014).

[28] R. A. Malfiet and J. A. Tjon, Nucl. Phys. A **127**, 161 (1969).

[29] S. Veerasamy and W. N. Polyzou, Phys. Rev. C **84**, 034003 (2011).

[30] J. Carbonell, J.-M. Richard, and S. Wycech, Z. Phys. A: Hadrons Nucl. **343**, 325 (1992).

[31] T.-A. Shibata, Phys. Lett. B **189**, 232 (1987).

[32] J. Carbonell, G. Ihle, and J.-M. Richard, Z. Phys. A **334**, 329 (1989).

[33] J. Haidenbauer, T. Hippchen, K. Holinde, and J. Speth, Z. Phys. A **334**, 467 (1989).